ARCHIVES OF ELECTRICAL ENGINEERING VOL. 71(4), pp. 1017–1034 (2022)

DOI 10.24425/aee.2022.142122

Research on dual-mode switching of the new dual full-bridge topology of the beam supply

CHANGZU AN[1], HONGXIA LU[2]

[1]*CCCC Ruitong Road & Bridge Maintenance Technology Co. Ltd. China*

[2]*Xi'an Railway Vocational & Technical Institute China*

e-mail: anchangzu@163.com

(Received: 5.06.2022, revised: 13.07.2022)

Abstract: In order to meet the operation requirements of the beam supply with multi-working conditions, multi-modes and high efficiency, a dual-mode hybrid output control method combining phase-shifting and pulse-width dual-mode modulation technology with secondary side series-parallel operation is proposed. In this paper, the structure and working mode of the new dual full-bridge topology are firstly analyzed. Secondly, the main circuit parameters are designed according to the power performance indicators, and the losses under two control modes of phase shift and pulse width are calculated. Finally, comparing the losses of these two control methods, and combining the series-parallel operation mode of the secondary side of the transformer, a dual-mode switching control method of the beam supply is designed. In order to verify the rationality of the dual-mode mixed output control method, a principle prototype with a rated capacity of 2 kW, a rated voltage of 1 800 V and a switching frequency of 50 kHz was used for verification. Experiments show the effectiveness and superiority of the dual-mode hybrid output control method.

Key words: beam supply, dual full-bridge converter, duty cycle control, ion electric propulsion, phase shift control

1. Introduction

With the rapid development of high-power ion-electric propulsion technology in China, the power level of the ion thruster power processing unit (PPU) is getting higher and higher, and the beam supply with high efficiency and high power density has been the goal of PPU development.

The internal structure of the PPU is shown in Fig. 1. The beam supply provides electrical power for the PPU optical components, so that the inert plasma is drawn out at a high speed, thereby generating reverse thrust to adjust the operating attitude of the spacecraft in space. As the core component of the PPU, the beam supply makes its output efficiency optimal within the full power range, which is the key to achieving high-efficiency and high-power density [1]. Therefore, improving the output efficiency of the beam supply is of great significance to the rapid development of the high-power ion electric propulsion technology in China [2].

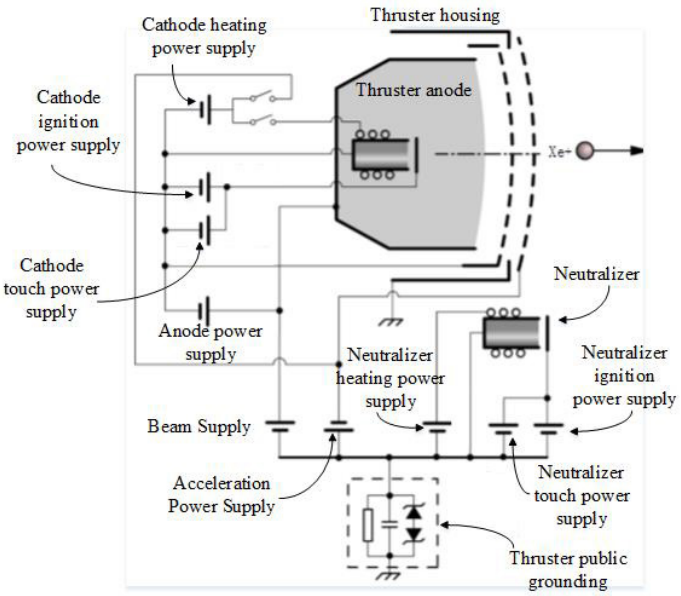

Fig. 1. PPU structure diagram

At present, according to different application environments, the improvement of the beam supply in the world is mainly in topology and control methods, and the optimization of efficiency is particularly insufficient [3]. Astrium's ion thruster beam supply consists of two sets of converters. The main converter is a resonant DC/DC topology, and the secondary converter is a push-pull topology, which has limited voltage regulation capability and cannot control the system current. The "Deep Space No. 1" thruster beam supply adopts a non-resonant full-bridge circuit, which can meet the requirements of a wide dynamic range and high power, but the heat consumption will reduce the efficiency of the PPU. The beam supply of the domestically developed LIPS-200 ion thruster is composed of a set of full-bridge hard-switching DC/DC conversion circuits. The next-generation LIPS-300 thruster is designed on the basis of the LIPS-200 thruster. The adjustment range of its output voltage needs to be further improved [4]. At present, the control signal of the beam supply adopts the phase-shift control signal and the duty cycle control signal. Phase shift control is easy to achieve soft switching and improve efficiency under heavy load, and the current is small under light load, which does not meet the soft switching condition. The conduction loss of duty cycle control is only in the energy transmission stage, and the efficiency of duty cycle

control is higher at light load [5]. Therefore, it is necessary to design a control method that meets the optimal efficiency in the full power range of the system [6].

Aiming at the technical requirements of a wide-range voltage output under the conditions of a wide-range voltage input of the beam supply, this paper proposes a dual-mode switching strategy of a new dual-full-bridge topology of the beam supply based on the original full-bridge topology. This switching strategy utilizes the series-parallel operation of the secondary windings of the power transformer in the new dual full bridge, and combines the advantages of phase-shift control and duty-cycle control. Finally, the output voltage can be adjusted in a wide range, and the output efficiency of the beam supply can be optimized in the full power range.

2. New topology and working principle of beam supply

2.1. Topology of the converter

The new dual full-bridge topology of the beam supply is shown in Fig. 2. The A-bridge is composed of A1, A2, A3, A4 power metal oxide semiconductor field effect transistors (MOSFETs) and transformers. It is a full-bridge circuit. The B-bridge is composed of B1, B2, B3, B4 power MOSFETs and transformers, and it is also a full-bridge circuit. After the rectifier bridge, the alternating current of the transformer secondary windings of the A bridge and the B bridge becomes direct current. Because the adjacent bridge arms of the two rectifier bridges have the same function, the topology can be simplified as a three-arm rectifier bridge, as shown in Fig. 1. The characteristic of this topology is to realize two operation modes of T1 and T2 secondary side parallel and series [7]. The structure of input parallel and output series and parallel can effectively reduce the current stress of the MOSFET and the capacity of transformers, and under the conditions of variable thrust, it can meet the requirements of a wide-range output of beam supply voltage to the greatest extent [8].

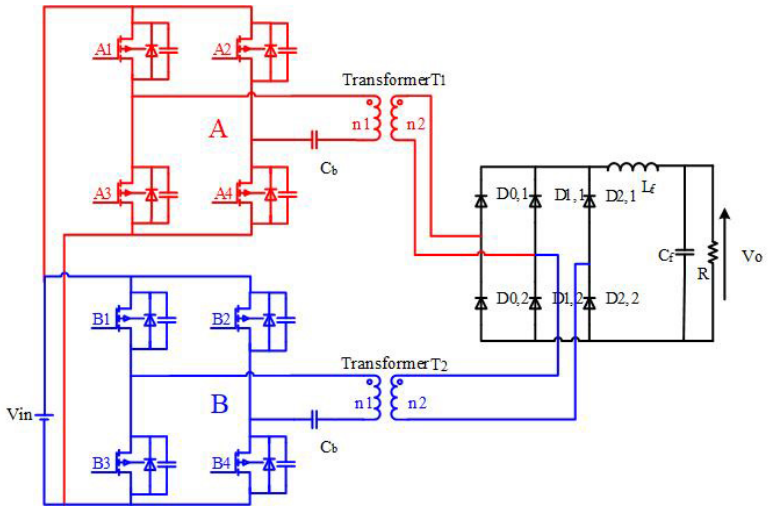

Fig. 2. New dual full-bridge circuit topology

2.2. The working modal analysis of the converter

For ease of understanding, it is assumed that the power MOSFETs are ideal devices and the two transformers have the same turns ratio.

Mode A $(t_0 - t_1)$

As shown in Fig. 3, A1, A4, B1, and B4 are turned on, the input currents of the A bridge and the B bridge begin to be transmitted to the secondary windings of the two transformers, and the primary currents I_{p1} and I_{p2} of T_1 and T_2 begin to increase linearly. The diodes $D_{0,1}$, $D_{1,1}$, $D_{1,2}$ and $D_{2,2}$ are turned on and participate in the power conversion process, until the cathode voltage of $D_{1,1}$ and $D_{1,2}$ is higher than the anode voltage, which makes $D_{1,1}$ and $D_{1,2}$ reversely cut off [9].

Mode B $(t_1 - t_2)$

When the circuit is running, mode A lasts for a short time and then enters mode B, as shown in Fig. 4. A1, A4, B1 and B4 are still turned on. At this time, $D_{1,1}$ and $D_{1,2}$ are turned off, but $D_{0,1}$ and $D_{2,2}$ are still turned on. The secondary coils of the transformer are connected in series. The primary side currents of T_1 and T_2 continue to rise, and the secondary side windings enter the true series mode. At this time, the output port voltage V_o is the sum of the port voltages of T_1 and T_2.

$$\begin{aligned} I_{p1} &= I_{p2}\,, \\ V_o &= V_{\text{sec}\,1} + V_{\text{sec}\,2} - V_{D_{0,1}} - V_{D_{2,2}} = 2\left(V_{\text{sec}\,1} - V_{D_{0,1}}\right), \end{aligned} \tag{1}$$

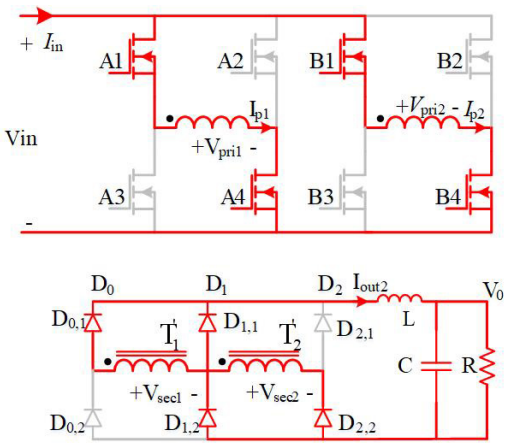

Fig. 3. Simplified diagram of mode A

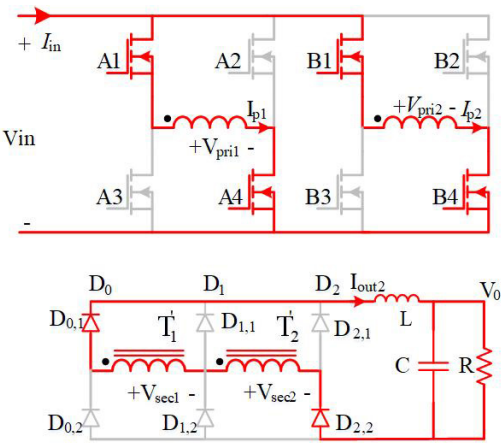

Fig. 4. Simplified diagram of mode B

Mode C $(t_2 - t_3)$

As shown in Fig. 5, A1 and A4 are turned off, and B1 and B4 are still turned on. Through the resonant circuit composed of the primary leakage inductance L_{1k} of T_1 and the parasitic capacitance C_{oss} of the power MOSFET, the primary current of T_1 decreases slowly, and T_2 still

participates in power conversion. Because the voltage of the secondary winding of T_2 remains unchanged, the voltage of the secondary winding of T_1 continues to decrease, which causes the diodes $D_{0,1}$ and $D_{1,2}$ to be reversely cut off, and $D_{1,1}$ and $D_{2,2}$ are still on. At this time, the secondary windings of T_1 and T_2 are in a series-to-parallel transition state.

The parasitic capacitance voltage of the power MOSFET is:

$$V_{C_{\text{oss}}} = nI_o Z_o \sin \omega_o (t - t_3) . \tag{2}$$

Among them,

$$\omega_o = \frac{1}{\sqrt{2L_{1K}C_{\text{oss}}}} Z_o = \sqrt{\frac{L_{1K}}{2C_{\text{oss}}}} .$$

Mode D $(t_3 - t_5)$

As shown in Fig. 6, B1, B4, A2 and A3 are turned on. When B1 and B4 are turned on, the voltage of the primary winding of T_2 is positive on the left and negative on the right. When A2 and A3 are turned on, the voltage on the primary winding of T_1 is negative on the left and positive on the right. Therefore, the primary currents flowing through the two transformers are in opposite directions. At the same time, the secondary coils of T_1 and T_2 are in a parallel state. At this time, the current flowing through $D_{1,1}$ is twice the current flowing through $D_{0,2}$ and $D_{2,2}$ and the output port voltage is equal to the T_1 and T_2 port voltages.

$$\begin{aligned} I_{p1} &= -I_{p2} , \\ V_o &= V_{\text{sec}\,1} - V_{D_{0,2}} - V_{D_{1,1}} = nV_{\text{pri}\,1} - 2V_{D_{1,1}} . \end{aligned} \tag{3}$$

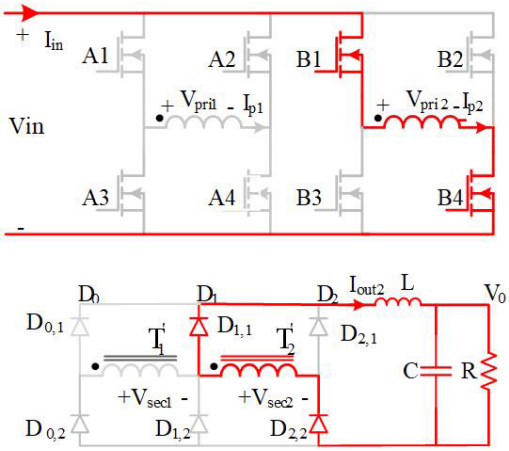

Fig. 5. Simplified diagram of mode C

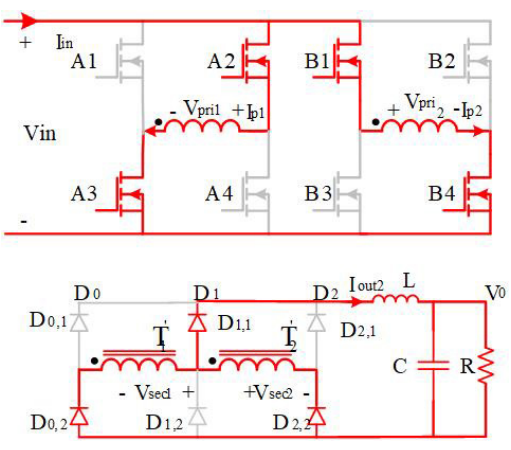

Fig. 6. Simplified diagram of mode D

Mode E $(t_5 - t_6)$

As shown in Fig. 7, A2 and A3 are still turned on, B1 and B4 are turned off. At this time, the primary current of T_2 decreases through the resonant circuit, which is similar to mode C.

T_1 participates in power conversion. Because the voltage on the secondary side of T_1 remains unchanged, the voltage on the secondary side of T_2 continues to decrease, which causes the diode to be turned off, and the diodes $D_{1,1}$ and $D_{0,2}$ to be turned on, thus entering the next moment, and the process from A to D will be repeated, but the current direction is opposite.

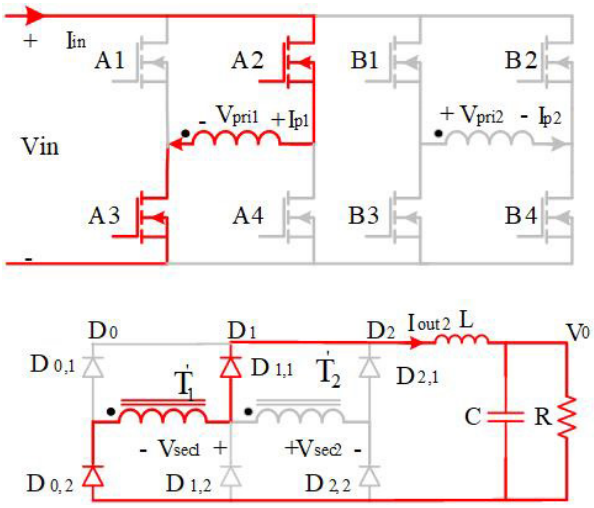

Fig. 7. Simplified diagram of mode E

For the new dual full-bridge topology, the relationship between V_{in} and V_o can be expressed as:

$$M(D) = \frac{V_o}{V_{\text{in}}} = 2nD,$$
$$D = \frac{(T_s - 2T_{\text{dead}} - T_\theta)}{T_s}, \tag{4}$$

where T_{dead} is the dead time between A1 and A2, T_θ is the phase shift angle time and T_s is the switching period.

By analyzing the change from mode A to mode D, the time series waveform is obtained, as shown in Fig. 8. Under different phase shift angles, the output voltage V_o will change continuously from $nv_{\text{pri}\,1} - 2v_{D_{0.1}}$ to $2nv_{\text{pri}\,1} - 2v_{D_{0.1}}$. If assuming that the conduction voltage of the diode drops to zero, the maximum value of the output voltage is twice the minimum value. Therefore, when the output voltage is high, in order to reduce the capacity of each transformer, the secondary sides of the two transformers are connected in series. When the output voltage is low, in order to reduce the current flowing through each transformer, the secondary sides of the two transformers are connected in parallel, which enables wide-range output voltage regulation under wide-range input voltage conditions [10].

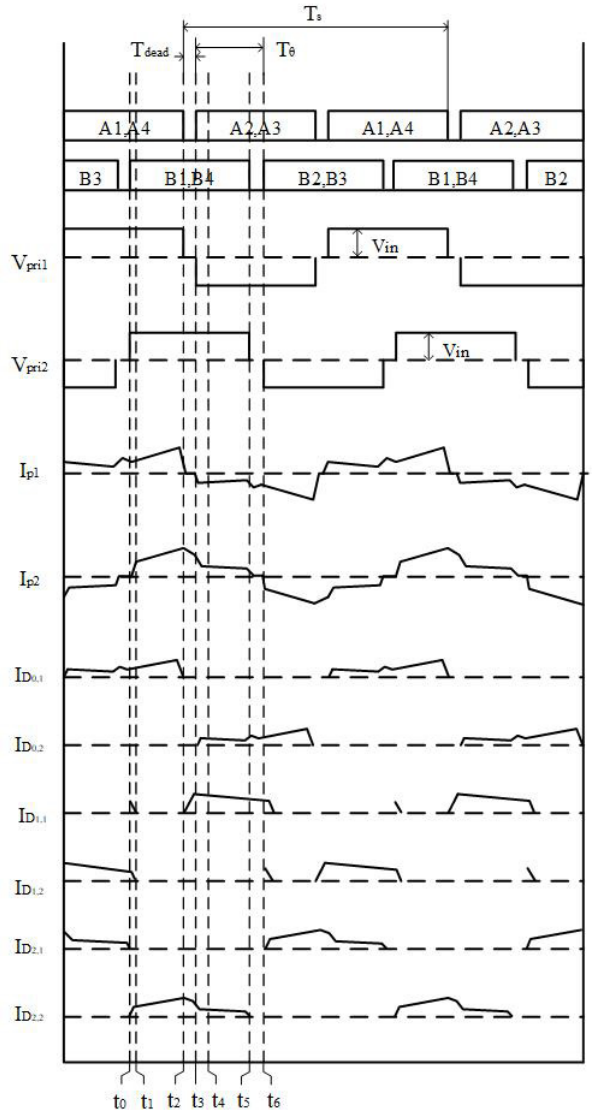

Fig. 8. Time series waveform

3. Parameter design and loss comparison

3.1. Converter parameters design

1. Selection of inverter bridge power MOSFET

Because the primary side of the new dual full-bridge topology transformer is two inverter bridges in parallel, and the DC bus voltage varies from 80 to 160 V, the maximum voltage $V_{\text{in\_max}}$ that the main power MOSFET can withstand is 160 V when it is turned off. Taking into account

Table 1. Full bridge converter parameters

Parameter name	Symbol	Value	Unit
Input DC voltage	V_{in}	80–160 (standard conditions 100)	V
Output DC voltage	V_o	175–1800	V
Output DC current	I_o	< 1.3	A
Transformer ratio	K	1/10	
Switching frequency	f_s	50	kHz
Load resistance	R	2 000	Ω
T leakage inductance	L_r	0.6	μH
Filter capacitor	C_f	6.1	μF
Filter inductor	L_f	500	μH

the voltage spikes generated during the turn-on and turn-off process, the withstand voltage value of the power MOSFET of the inverter bridge is chosen to be twice $V_{\text{in\_max}}$. The maximum power P_{o_max} of single-circuit overload is 1 000 W, and the minimum voltage $V_{\text{in\_min}}$ of the DC bus is 80 V, then the maximum effective current of the single-circuit DC bus is:

$$I_{\text{in\_max}} = \frac{P_{o\_\text{max}}}{\eta V_{\text{in\_min}}} . \tag{5}$$

According to the formula, the maximum current is 26 A, and the designed switching frequency of the converter is 50 kHz. Therefore, the power MOSFET in the system design adopts the IPA60R099C6 (37.9 A@25°C 600 V 99 mΩ) power MOSFET.

The maximum value of 26 A is obtained, and the converter design switching frequency is 50 kHz. So, the system design uses the IPA60R099C6 (37.9 A@25°C 600 V 99 mΩ) power MOSFET for the power MOSFET [11].

2. Rectifier diode selection

The secondary side of the transformer is a three-bridge rectifier structure. When the secondary side of the transformer is in parallel mode, the reverse voltage applied to the middle rectifier bridge arm is twice that of the other two bridge arms. Therefore, according to the specific parameters of the converter design, the maximum reverse voltage $V_{Dr} = (V_{\text{in}}/K) \times 2$ applied to the rectifier diode is 3 200 V, and the three-arm rectifier bridge operates in a hard-switching state. Affected by the parasitic parameters in the loop and the reverse recovery of the diode, a sufficient margin should be left for the selection of the diode [12].

In one switching cycle, regardless of whether the secondary side of the transformer is in series mode or parallel mode, the operation of the three-arm rectifier circuit is as follows:

a. When there is voltage on the secondary side of the two transformers, the three-arm rectifier bridge has a rectification function. At this time, the maximum current flowing through the rectifier bridge is the maximum load current, $i_{DR(\text{max})} = I_{o(\text{max})} = 1.3$ A.

b. When the voltage on the secondary side of the transformer drops to zero, all the three-arm rectifier tubes are turned on, and it is considered that the currents flowing through each tube are equal, and they are all one-third of the load current. Therefore, the maximum current flowing through each bridge arm is: $i_{DR(\max)} = I_{o(\max)} + \Delta I_{Lf}/3 = 1.387$ A.

The selection of the output rectifier mainly considers the withstand voltage value. The forward voltage drop of the high withstand voltage rectifier is large, which leads to an increase in the power consumption of the device and puts forward higher requirements for the heat dissipation design of the system. Therefore, according to the reverse voltage and on-current at both ends of the diode, compared with the Schottky diode, the DSEI30 type fast recovery diode is selected, which has a lower forward voltage drop and a shorter reverse recovery time. Its voltage rating is 1 200 V, and its current rating is 26 A. In the actual circuit, in order to achieve a maximum reverse voltage of 3 600 V, three diodes are connected in series.

3. Selection of DC blocking capacitors

In order to effectively solve the problem that the DC component is generated on the primary side of the transformer due to the different characteristics of the power MOSFET, and then the magnetic core of the transformer is biased, this paper decides to connect a DC blocking capacitor in series on the primary side of the transformer [13].

The selection of DC blocking capacitors mainly depends on two factors:

i. In order to make the effective value of the duty cycle $D_{\text{eff max}}$ of the secondary side of the transformer larger, the value of C_b should be smaller;
ii. In order to reduce the reverse voltage of the lagging bridge arm, the value of C_b should be larger.

When the system output is fully loaded, the voltage peak value of the DC blocking capacitor is: $V_{Cb\_\max} = 20\%V_{\text{in}}$, and the value range of the shunt capacitance of the MOSFET is: $C_r \gg C_b$, in summary, the calculation formula of the DC blocking capacitor is:

$$C_b = \frac{I_{p\_\max} \times T_{\text{on}}}{2V_{Cb\_\max}} = \frac{I_{p\_\max} D}{4 f_s V_{Cb\_\max}}. \tag{6}$$

In the formula, $V_{Cb\_\max}$ is the peak voltage of the DC blocking capacitor, $I_{p\_\max} = 13$ A is the peak current of the primary side of the transformer, the maximum value of D is 0.46, and the design switching frequency of the power supply is: $f_s = 50$ kHz. Based on this, the value of the DC blocking capacitor can be obtained as: $C_b = 2.99$ µF. Because the DC blocking capacitor needs to withstand a high current of 13 A on the primary side of the transformer, and needs to have a faster charging and discharging speed, therefore, a 4.7 F film capacitor is selected as the DC blocking capacitor. This DC blocking capacitor has less loss, good temperature characteristics, and can withstand higher peak currents.

4. Selection of output filter inductor

The function of the output filter in the full-bridge converter is to filter out the harmonic components generated by the inverter bridge. If the inductance of the output filter is larger, the filtering effect is more obvious and the ripple is smaller. However, in practical applications, it is necessary to consider the volume, weight, and filter time constant of the filter circuit, as well as the impact on the system stability when closed-loop control is used. Therefore, the design filter time

constant needs to be comprehensively considered. After passing through the two transformers and the three-arm rectifier bridge, the AC square wave voltage generated on the primary side of the converter outputs the DC voltage with high frequency harmonic components, the operating frequency of the secondary side rectifier is twice the operating frequency of the primary side inverter.

The current ripple of the filter inductor in the converter is:

$$\Delta I_{L_f} = \frac{V_{\text{out}}}{2 \times 2 f_s L_f} \left(1 - \frac{V_{\text{out}}}{\frac{V_{\text{in}}}{K} - V_{L_f} - V_D} \right). \tag{7}$$

In order to reduce the pulsation of the output filter inductor current, a larger filter inductor value should be selected, but the volume, weight, and cost of a large inductor are relatively high, and affect the dynamic response speed of the closed-loop control. Therefore, the pulsating current of the output filter inductor takes 20% of the maximum output current, and Eq. (7) can be transformed into the following equation:

$$L_f = \frac{V_{\text{out}}}{2 \times 2 f_s \times 20\% I_{o\_\max}} \left(1 - \frac{V_{\text{out}}}{\frac{V_{\text{in}}}{K} - V_{L_f} - V_D} \right). \tag{8}$$

Since the design requirement of the beam power supply is to realize a wide range of voltage output under the condition of a wide range of voltage input, in order to ensure that the maximum value of the pulsating current of the output filter inductor does not exceed $20\% \cdot I_{o\_\min}$, V_{out} takes $V_{\text{out\_min}}$, V_{in} takes $V_{\text{in\_min}}$, and $L_f = 500$ µH can be obtained by substituting these two values into Eq. (8).

5. Selection of output filter capacitors

The selection of the filter capacitor depends on the peak value $\Delta V_{\text{out\_}pp}$ of the output voltage of the converter, and the output filter capacitor value can be calculated according to Formula (9).

$$C_f = \frac{V_{\text{out}}}{8 L_f \times (2 f_s)^2 \times \Delta V_{\text{out\_}pp}} \left(1 - \frac{V_{\text{out}}}{\frac{V_{\text{in}}}{K} - V_{L_f} - V_D} \right). \tag{9}$$

Among them, V_{out} takes $V_{\text{out\_min}}$ and V_{in} takes $V_{\text{in\_max}}$, thus $C_f = 6.1$ µF.

For switching power supply output filter capacitors, large-capacity electrolytic capacitors are generally used. Considering that electrolytic capacitors have equivalent series resistance (ESR), the use of multiple electrolytic capacitors in parallel can effectively reduce ESR and reduce output ripples. The withstand voltage value of the output filter capacitor depends on the maximum value of the output voltage. Considering factors such as cost and volume, the withstand voltage value is generally selected to be slightly higher than the output voltage. Due to the unstable high-frequency characteristics of electrolytic capacitors, the high-frequency current components applied to both ends of the electrolytic capacitor cannot be absorbed. Therefore, a high-frequency capacitor should be connected in parallel at both ends of the electrolytic capacitor, generally 10 nF or 100 nF.

3.2. Loss calculation for two control methods

1. Loss calculation of inverter unit

The MOSFET model used in the inverter bridge is IPA60R099C6, and its loss consists of on-state loss and switching loss [14].

When phase-shift control is adopted, the loss of the MOSFET is mainly in the power transmission stage and the internal circulation stage [15], and the effective value of the current flowing through the MOSFET in the power transmission stage is as in Eq. (10):

$$I_{\text{energy\_rms}} = \sqrt{\frac{1}{T_s}\int_0^{DT_s}\left(i_p(t_0) + \frac{i_p(t_1) - i_p(t_0)}{DT_s}\right)^2 \mathrm{d}t} = \sqrt{D}\sqrt{\frac{I_{p1}^2 + I_{p1} \times I_p + I_p^2}{3}}\,. \tag{10}$$

The conduction loss is calculated by Eq. (11):

$$P_{\text{con\_mos}} = I_{\text{energy\_rms}}^2 R_{\text{DS(on)}}\,. \tag{11}$$

The effective value of current flowing through the MOSFET in the internal circulation stage is shown in Eq. (12):

$$\begin{aligned} I_{\text{cir\_rms}} &= \sqrt{\frac{1}{T_s}\int_{DT_s}^{T_s/2}\left(i_p(t_1) + \frac{i_p(t_1) - i_p(t_4)}{(1-2D) \times T_s/2}\,(t - DT_s)\right)^2 \mathrm{d}t} \\ &= \sqrt{\frac{1-2D}{2}}\sqrt{\frac{I_{p2}^2 + I_{p2} \times I_p + I_p^2}{3}}\,. \end{aligned} \tag{12}$$

The internal circulation stage loss $P_{\text{mos\_diode}}$ is calculated by (13):

$$P_{\text{mos\_diode}} = I_{\text{cir\_rms}} V_{DF}\,. \tag{13}$$

When duty cycle control is used, the losses of the MOSFET mainly occur in the power transfer stage and in the turn-on and turn-off process, and the switching losses are calculated by Eqs. (14) and (15):

$$E_{\text{sw\_on}} = \frac{1}{2}\int_0^{t_{d(\text{on})}+t_r} v_{\text{DS}}(t) i_p(t)\,\mathrm{d}t, \tag{14}$$

$$E_{\text{sw\_off}} = \frac{1}{2}\int_0^{t_{d(\text{off})}+t_r} v_{\text{DS}}(t) i_p(t)\,\mathrm{d}t, \tag{15}$$

where the area of $v_{\text{DS}} \times i_p$ is the power of the switch, the time integral of which is the switching energy, so the formula for calculating the switching loss is as in Eq. (16):

$$P_{\text{sw\_mos}} = (E_{\text{sw\_on}} + E_{\text{sw\_off}})\, f_s\,. \tag{16}$$

Substituting the data corresponding to the datasheet, the total loss of the MOSFET can be calculated [16].

2. Loss calculation of rectifier bridge arm

The three-bridge arm rectifier bridge adopts a DSEI30-type fast recovery diode, the conduction voltage drop is $V_F = 2.55$ V ($T_{VJ} = 25°$), and the loss is calculated as in Eq. (17):

$$P_{\text{con\_diode}} = I_{\text{diode\_rms}} V_F \,. \tag{17}$$

According to the calculation of the losses, it can be seen that the losses of the new dual full-bridge topology are mainly concentrated on the power MOSFET and rectifier parts, and the main purpose of this paper is to compare the efficiency advantages of phase-shift control and duty cycle control, and design a dual-mode control method combining the advantages of the two control methods, and finally achieve the best efficiency in the full power range. Figures 8 and 9 depict the losses corresponding to each power point under phase shift control and duty cycle control, respectively, and the output efficiency corresponding to different power points shown in Fig. 10 can be derived from Figs. 9 and 10.

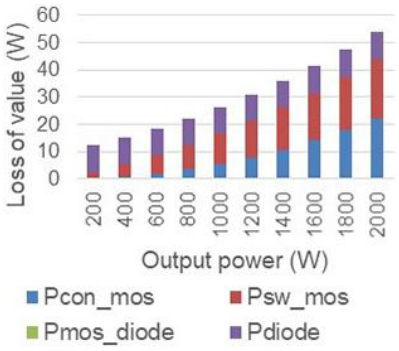

Fig. 9. Loss distribution under phase shift control

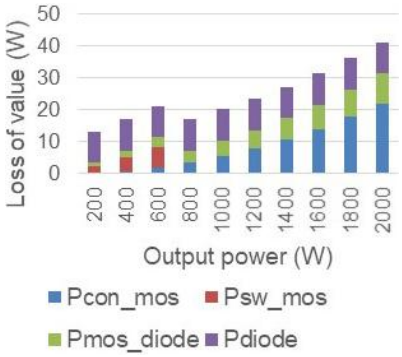

Fig. 10. Loss distribution under duty cycle control

3. Calculation of Transformer Loss P_{tr}

Transformer loss is divided into two parts: copper loss and iron loss. Iron loss is the loss of the ferrite core, and copper loss is the coil conduction loss.

4. Calculation of output filter inductor loss P_{Lf}

As can be seen in Fig. 11, the output efficiency of duty cycle control is higher than that of phase shift control under light load conditions, and the output efficiency of phase shift control is higher than that of duty cycle control in heavy load conditions [17]. Because soft switching cannot be achieved under light load conditions and the phase-shift control produces circulating current loss, the loss of phase-shift control is higher than that of duty cycle control. In heavy-load conditions, phase-shift control realizes soft switching, which greatly reduces losses and makes phase-shift control have more efficiency advantages [18].

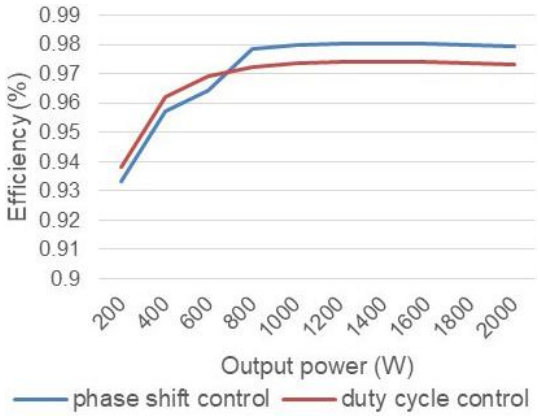

Fig. 11. Output efficiency comparison

4. Dual-mode hybrid output control design

According to the modal analysis of the converter operation, it is known that the primary side control signal of the new double full bridge topology can use phase shift control and duty cycle control, and the secondary side of the transformer can operate in series mode and parallel mode. As shown in Table 2, this paper combines the advantages of two control modes and two operation modes to achieve a wide range of output voltage regulation under wide range input voltage conditions and optimal efficiency in the full power range.

Table 2. Combination of control mode and operation mode

Operation model	**Control way**	
	Phase shift control	**Duty cycle control**
Secondary side series operation	Phase-shift control series operation mode. In this mode, the system outputs high voltage and the corresponding output power is also larger. It is easy to implement soft switching technology and improve system operation efficiency.	Duty cycle control series operation mode, in this mode the system outputs high voltage, the corresponding output power is smaller, and the duty cycle control efficiency is higher
Secondary side parallel operation	Phase-shift control parallel operation mode. In this mode, the output voltage of the system is low, but the output power is large and it is easy to achieve soft switching. Phase-shift control has more efficiency advantages.	Duty cycle control parallel operation mode. In this mode, the system outputs low voltage, the corresponding output power is also smaller, and the duty cycle control efficiency is higher.

The system control switching process is shown in Fig. 12. The phase shift control and duty cycle control are switched according to the output power of the system, and the optimal switching

point of efficiency is selected according to the output efficiency curve shown in Fig. 10. The secondary side of the transformer performs series-parallel switching according to the output voltage, and the switching point voltage selects the maximum output voltage of the transformer.

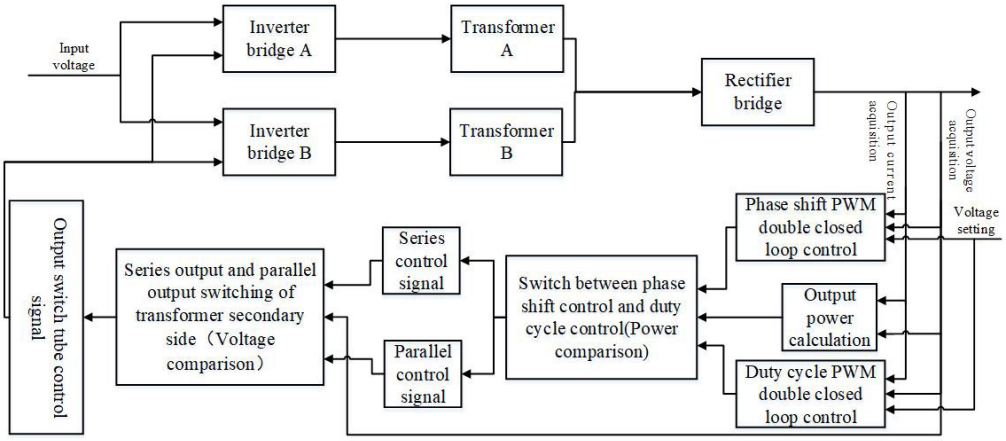

Fig. 12. System control switch

5. Experimental verification

In order to verify the mixed output control effect of the new dual full-bridge topology mode of the beam supply, a 2 000 W principle prototype is designed and completed. The normal working input voltage is 100 V under standard conditions, and the output voltage is 275−1 800 V. The system control switching is realized by programming. The main parameters are shown in Table 1. The output series-parallel switching point voltage is selected to be 800 V, and the optimal efficiency switching point is 800 W.

Figures 13(a) and 13(b) are the drive waveforms of duty cycle control and phase shift control, respectively, where channel 1 is the drive waveform of power MOSFET A1, channel 2 is the drive waveform of power MOSFET A4, power MOSFET A1 and A4 are diagonally positioned. During duty cycle control, A1 and A4 are turned on and off at the same time. During phase shift control, A1 leads A4. The control signal is adjusted by changing the magnitude of the phase difference. Figure 13(c) shows the process of switching from duty cycle control to phase shift control. As the output power increases, the system control switches from duty cycle control to phase shift control.

Figures 14(a) and 14(b) show the waveforms of series and parallel operation on the secondary side of the phase shift control, channels 1 and 2 are the driving waveforms of power MOSFET A1 and A4, respectively, channels 3 and 4 are the input square waves of transformers T_1 and T_2, respectively. It can be seen from Fig. 14(a), power MOSFET A1 and A4 are in the phase shift state at this time, the voltage direction of both ends of T_1 and T_2 is the same. According to the analysis in Section 2.2, it can be seen that the secondary sides of T_1 and T_2 operate in series. In

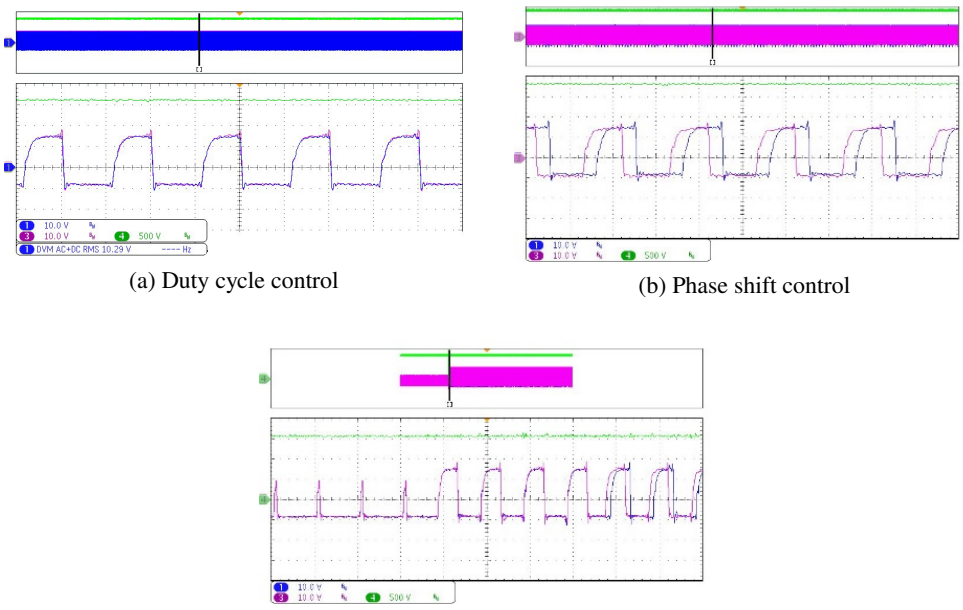

(a) Duty cycle control

(b) Phase shift control

(c) Duty cycle control to phase shift control switching process

Fig. 13. Two kinds of control mode waveform and switching process

Fig. 14(b), the voltage directions at both ends of T_1 and T_2 are opposite, so the secondary sides of T_1 and T_2 operate in parallel mode.

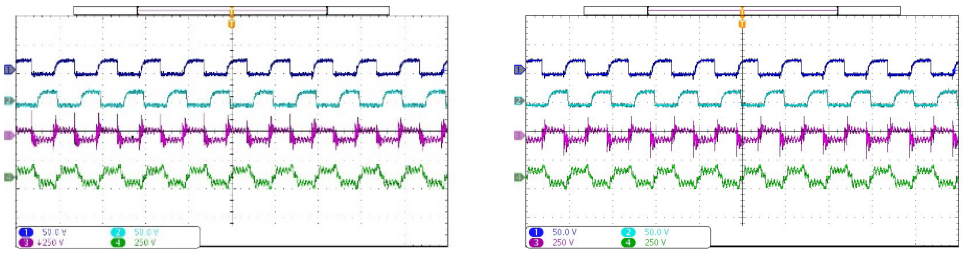

(a) Secondary side series operation

(b) Secondary side parallel operation

Fig. 14. The phase shift controls the secondary side series and parallel operation

Figures 15(a) and 15(b) are the waveforms of the series-parallel operation of the secondary side under duty ratio control, respectively. It can be seen from Fig. 15(a) that power MOSFET A1 and A4 are turned on and off at the same time, and the voltage directions at both ends of T_1 and T_2 are the same, which indicates that the system is in the duty cycle control series operation mode.

It can be seen from Fig. 15(b) that the voltage directions at both ends of T_1 and T_2 are opposite, and the system is in the duty cycle control parallel operation mode.

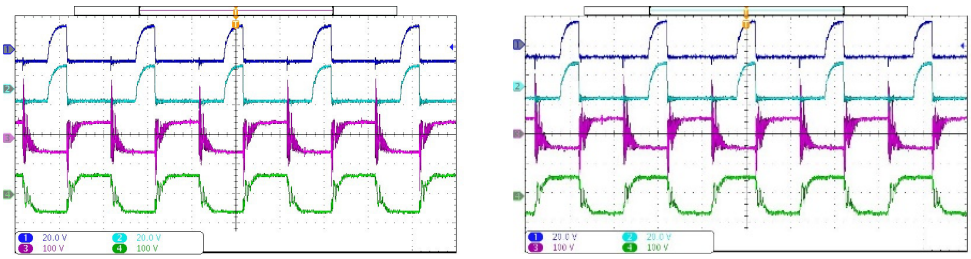

(a) Secondary side series operation (b) Secondary side parallel operation

Fig. 15. Duty cycle control secondary side series and parallel operation

Figures 16(a) and 16(b) show the process of a sudden increase and sudden decrease of the output voltage, respectively. It can be seen from Fig. 16(a) that the voltage suddenly increases from 500 V to 1 100 V, the secondary side switches from parallel to series, and when the voltage rises to about 800 V, the control mode is switched from duty cycle control to phase shift control. It can be seen from Fig. 16(b) that the output voltage suddenly decreases from 1 200 V to 800 V, and the secondary side switches from series to parallel. During this process, the series-parallel and control modes can be switched smoothly to meet the system stability requirements.

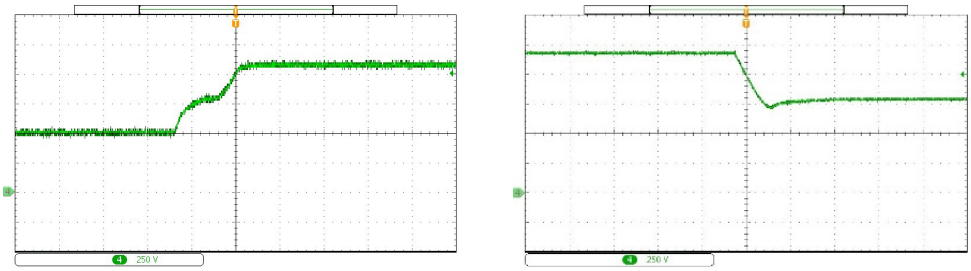

(a) Sudden increase of output voltage (b) Sudden decrease of output voltage

Fig. 16. Output voltage mutation

6. Conclusions

This paper proposes a new dual full-bridge topology structure of the beam supply. According to the topology characteristics, the series-parallel operation of the secondary side of the transformer is combined with the phase-shift and pulse-width dual-mode modulation technology, and a 2 000 W principle prototype is designed. The following conclusions are drawn:

1. In the new dual full-bridge topology, the series-parallel operation of the secondary side of the transformer can meet the wide-range voltage output under the wide-range voltage

input conditions of the beam supply, and can flexibly adapt to the power input and output requirements, while meeting the multi-working conditions and multi-mode operation of the thruster.

2. The combination of series-parallel operation on the secondary side of the transformer and the dual-mode modulation technology of phase shift, as well as pulse width, keep the power supply system in the full power range with optimal efficiency, the heat consumption is small, and the overall efficiency of the system is improved.
3. Through the 2 000 W prototype test, the secondary side series-parallel operation and phase shift/pulse-width dual-mode control can be switched smoothly, which can meet the system stability requirements.
4. The effective improvement of the output efficiency of the beam supply can further improve the power level of the ion electric propulsion system, and better meet the needs of deep space exploration tasks such as spacecraft orbit change, constant position, attitude adjustment, and resistance compensation.

References

[1] Bo Y., Jiao J., *Investigation of a New Micro-Nano Propulsion Concept*, Journal of Propulsion Technology, vol. 39, no. 6, pp. 1434–1440 (2018), DOI: 10.13675/j.cnki.tjjs.2018.06.029.

[2] Daren Y., Lei Q., Wenjia J., *China Electric power promotes the development and prospect of technology*, Journal of Propulsion Technology, vol. 41, no. 1, pp. 1–11 (2020), DOI: 10.13675/j.cnki.tjjs.190140.

[3] Zhicheng Z., Jun G., *All-electric propulsion research on the development of CEO satellite platform*, Spacecraft Engineering, vol. 24, no. 2, pp. 1–6 (2015), DOI: 10.3969/j.issn.1673-8748.2015.02.001.

[4] Chengqi L., Zuo G., *Analysis of Spacecraft Payload Capacity Based on Ion Propulsion System*, Journal of propulsion technology, vol. 40, no. 10, pp. 2183–2189 (2019), DOI: 10.13675/j.cnki.tjjs.180685.

[5] Brophy J., *The Dawn Ion Propulsion System*, Space Science Reviews, vol. 163, no. 1–4, pp. 251–261 (2011), DOI: 10.1007/s11214-011-9848-y.

[6] Weiren W., Wangwang L., *Investigation on the development of deep space exploration*, Science China (Technological Sciences), vol. 55, no. 4, pp. 1086–1091 (2012), DOI: 10.1007/s11431-012-4759-z.

[7] Hao Z., Haiying D., *Research on beam supply control strategy based on sliding mode control*, Archives of Electrical Engineering, vol. 69, no. 2, pp. 349–364 (2020), DOI: 10.24425/aee.2020. 133030.

[8] Qiang W., Bing L., *Novel Single-Phase Soft-Switching AC-DC-AC Converter*, Acta Electronica Sinica, vol. 48, no. 3, pp. 616–620 (2020), DOI: 10.3969/j.issn.0372-2112.2020.03.026.

[9] Qiang W., Yan X., *Soft switching voltage source inverter with parallel resonant DC link*, Acta Electronica Sinica, vol. 41, no. 11, pp. 2317–2320 (2013), DOI: 10.3969/j.issn.0372-2112.2013.11.033.

[10] Xuewen S., *Research on control Strategy of bidirectional DC-DC converter*, MA Thesis, School of Electrical Engineering, Beijing Jiaotong University, Bei Jing (2019), DOI: 10.26944/d.cnki.gbfju.2019.000381.

[11] Beiranvand R., Rashidian B., Zolghadri M.R., *A design procedure for optimizing the LLC resonant converter as a wide output range voltage source*, IEEE Transactions on Power Electronics, vol. 27, no. 8, pp. 3749–3763 (2012), DOI: 10.1109/TPEL.2012.2187801.

[12] Sucheng L., Qingqing L., *Formulation of General Large-signal Adaptive Control Strategy For DC-DC Converter*, Journal of Power Supply, vol. 16, no. 3, pp. 16–22 (2018), DOI: 10.13234/j.issn.2095-2805.2018.3.16.

[13] Kawahara K., Alfieri G., *Detection and depth analysis of deep levels generated by ion implantation in n-and p-type 4H-SiC*, Journal of Applied Physics, vol. 106, no. 1, pp. 713–719 (2009), DOI: 10.1063/1.3159901.

[14] Brett A.H., Joseph J.S., Michael J.O.L., *Performance and Stability of Large-Area 4H-SiC 10-kV Junction Barrier Schottky Rectifiers*, IEEE Transaction on Electron Devices, vol. 55, no. 8, pp. 1864–1870 (2008), DOI: 10.1109/TED.2008.926655.

[15] Feng H., *Digital- controlled transfer full - bridge soft - switching converter*, MA Thesis, School of Electrical Engineering, Nanjing University of Aeronautics and Astronautics, Nan Jing (2004), DOI: 10.7666/d.y580275.

[16] Yanqiong S., Gang Y., *Analysis of the characteristics of the phase-shifting full-bridge DC/DC converter with isolating capacitance*, Power Electronics, vol. 39, no. 3, pp. 11–13 (2005), DOI: 10.3969/j.issn.1000-100X.2005.03.005.

[17] Miyake H., Kimoto T., Suda J., *Improvement of Current Gain in 4H-SiC BJTs by Surface Passivation with Deposited Oxides Nitrided in N_2O or NO*, IEEE Electron Device Letters, vol. 32, no. 3, pp. 285–287 (2011), DOI: 10.1109/LED.2010.2101575.

[18] Dhimish Mahmoud, Schofield Nigel, *Single-switch boost-buck DC-DC converter for industrial fuel cell and photovoltaics applications*, International Journal of Hydrogen Energy, vol. 47, no. 2, pp. 1241–1255 (2022), DOI: 10.1016/J.IJHYDENE.2021.10.097.